SAND2025-12966J

Geophysical Research Letters

RESEARCH LETTER
10.1029/2025GL116415

Key Points:
- Infrasound microbarometers capture diurnal and weekly cycles in ground wind speed and anthropogenic sound
- These site-specific noise levels vary substantially over sub-kilometer scales
- Microbarometer deployments provide insight into localized micrometeorology and trends in anthropogenic activity

Supporting Information:
Supporting Information may be found in the online version of this article.

Correspondence to:
A. K. Malach,
akbal@sandia.gov

Citation:
Malach, A. K., Bowman, D. C., Wharton, S., Turley, R. S., White, R. L., Schalk, W., & the PE1 Experiment Team (2025). Cyclic background noise variations on infrasound microbarometers from micrometeorology and human activity. *Geophysical Research Letters*, *52*, e2025GL116415. https://doi.org/10.1029/2025GL116415

Received 21 APR 2025
Accepted 15 SEP 2025

Cyclic Background Noise Variations on Infrasound Microbarometers From Micrometeorology and Human Activity

Amrit K. Malach[1], Daniel C. Bowman[1,2], Sonia Wharton[3], Reagan S. Turley[4], Robert L. White[4], Walter Schalk[5], and the PE1 Experiment Team[6]

[1]Sandia National Laboratories, Livermore, CA, USA, [2]Pacific Northwest National Laboratory, Chapel HIll, NC, USA, [3]Lawrence Livermore National Laboratory, Livermore, CA, USA, [4]Nevada National Security Sites, North Las Vegas, NV, USA, [5]National Atmospheric and Oceanic Administration—Special Operations and Research Division, North Las Vegas, NV, USA, [6]See Acknowledgments

Abstract Infrasound microbarometers deployed on the Earth's surface capture pressure fluctuations and acoustic signatures, revealing trends in surface wind speed and cycles in ambient sound. Previous studies investigated wind noise trends at quarter day resolution and urban acoustic background variations on hourly to weekly scales. Cyclic variations at sub-hourly resolution over local distances remain unaddressed. We show that topography-driven micrometeorology impacts diurnal background noise levels below 10 Hz. Anthropogenic noise occurs over daily and weekly cycles, with inputs from traffic, ventilation systems, and power lines. These noise patterns vary at stations spaced less than a kilometer apart. We observe these phenomena by using a circular spectrogram to visualize frequency trends over a periodic temporal scale. This study demonstrates that infrasound microbarometer deployments can highlight localized wind patterns and time scales of human activity. The results suggest that future microbarometer deployments may benefit from site noise surveys before selecting final sensor locations.

Plain Language Summary Low frequency sound sensors are exquisitely sensitive to minuscule pressure fluctuations. Wind generates strong signals on these sensors, which can be problematic when they overwhelm other signatures of interest. Human-generated low frequency sounds from turbines, machinery, vehicles, etc. are often detected as well. Both wind and human noise tend to fluctuate in a periodic fashion over days to weeks. Previous studies have investigated broad trends in these signatures. However, the time and space scales has not been examined in detail. We developed a visualization method that shows how these noise sources varied on daily to weekly scales. We found that both wind and human noise can be quite different even over short distances. This indicates that wind noise is sensitive to the time of day and very localized conditions. Most sources of human generated sound tended to be higher during work hours. Future sound sensor deployment planners should record background noise in the area before settling on a particular location.

1. Introduction

Energy released into the atmosphere can produce acoustic waves. These waves carry information about their origin, propagation path, and the properties of the medium through which they pass. Low frequency acoustic waves, typically in the <20 Hz, or "infrasound" range, can travel across the globe. Accordingly, they have an important role in the monitoring and detection of explosions (Koch & Pilger, 2019; Park et al., 2018) as well as the characterization of volcanic hazards (Ripepe et al., 2018) and a whole host of other natural and anthropogenic phenomena (Campus & Christie, 2010). Acoustic waves from distant events tend to be very low amplitude compared to pressure fluctuations generated by wind (Raspet et al., 2019) or local sound sources such as those caused by human activity (D. G. Albert & Decato, 2017). The ideal infrasound sensor site has low winds and lies far from anthropogenic interference, but this is often difficult to achieve in practice.

Researchers have conducted a series of studies on the impact of different terrain types and/or proximity to human activity on acoustic sensing. In their surveys of a global infrasound network, J. R. Bowman et al. (2005) and Brown et al. (2014) noted wide variability in background noise based on location and time of day, with the nighttime hours generally quietest. Macpherson et al. (2022) found that time of year, land cover, and even location of the sensor port with respect to nearby structures had a measurable effect on background noise levels of infrasound stations in Alaska. While urban areas have traditionally been considered unfavorable for geophysical acoustics equipment, Bird et al. (2021) found that anthropogenic signals typically did not extend below 8 Hz. Building on this result, Wynn and Dannemann Dugick (2023) showed that urban infrasound networks had noise levels comparable to those in more rural areas, at least at lower frequencies. Both studies also examined broadband urban infrasound trends versus time of day, noting that they seemed to correlate with diurnal wind patterns and human activity cycles.

It is presently unclear how global temperature rise and impacts to the jet stream due to climate change will affect ground wind speeds (Pryor et al., 2020), but human civilization will continue to use more and more energy for the foreseeable future (Zhang et al., 2023). Presumably, this will result in additional anthropogenic acoustic emissions over time. There has already been a measurable increase in ambient sound in the ocean over the last several decades due to human activity (Frisk, 2012). While some long-term background noise products have been generated for infrasound (Hupe et al., 2022), a systematic search for multi-year background noise trends has not been conducted. Thus, quantifying the micrometeorological, or local-scale meteorology (defined here to be scales less than 5 km per Wharton et al. (2023)), and anthropogenic drivers of infrasound background noise is key to understanding the present and future capabilities of geophysical acoustics as a means of monitoring natural and human-driven phenomena.

Here we present an analysis of infrasound and low audio range background noise recorded on a set of infrasound sensors in complex topography at various distances from facilities and roads. We investigate diurnal variations driven by micrometeorology as well as daily and weekly cycles due to human activity. We distinguish between wind interference and anthropogenic noise based both on frequency content and patterns of occurrence. This opens new avenues for understanding ground wind dynamics and human impact on the Earth's acoustic environment. Our study also provides a useful guide for researchers who are aiming to deploy their own networks in complex topographic settings and/or in areas with significant human activity.

2. Methods

An acoustic network was deployed to capture signals from the Physics Experiment 1 (PE1) at the Nevada National Security Site (NNSS) (Myers et al., 2024). The NNSS is an expanse of access-controlled land larger than the U. S. state of Rhode Island. The sensors used in this study are 40 km from the nearest public road and 60 km from the closest town, although they are located in proximity to active facilities and site roads. We focus on three non-seismically decoupled Hyperion IFSN-3100 series infrasound microbarometers recorded on REFTEK 130S digitizers at a sampling rate of 500 Hz. These microbarometers have a flat frequency response from 0.1 Hz to approximately 100 Hz. They were shielded from hydrodynamic noise using perforated wind domes, which reduces wind interference up to 7 dB over the 0.1–20 Hz frequency range (S. A. Albert et al., 2021). The stations examined in this study were located at the north end of a large valley called Yucca Flat (PER01), at a canyon entrance (PSDOR), and on a ridge (PSDNU; Figure 1).

These acoustic sensors were also located near active facilities and roads. PSDOR and PSDNU were a few hundred meters away from an underground complex excavated horizontally into the mesa to the north. The underground ventilation systems run Monday-Thursday at this facility. In addition, a small locomotive regularly enters and exits the tunnel during work hours on these days. Passenger vehicles, building ventilation systems, and heavy equipment are active Monday-Thursday as well. Station PER01 is located along an access road about half a kilometer from Area 12 Camp, a set of buildings typically occupied Monday-Thursday. All of these areas are access controlled, meaning that human activity follows the Monday-Thursday work week much more closely than it would in continuously occupied areas like cities.

We compiled data for each station during the month of November 2023 and then converted all data into Pascals. The resulting waveforms were divided into ten-minute sections for a total of 144 sections per day. Each ten-minute section was further divided into one-minute sections. A spectrum was generated for each of these one-minute sections using the multi taper method (Lees & Park, 1995). These one-minute sections were averaged together to produce a Welch spectrum for the 10 minute window. Any section containing a data gap was not included in the average. Ten-min sections corresponding to the same time of day were selected across the study period. Variations between workdays and weekends were of particular interest. Saturday and Sunday were considered weekends, whereas Wednesday and Thursday were selected as workdays. Representative spectra for weekends and weekdays were generated by taking the median for the same 10 min period across the selected

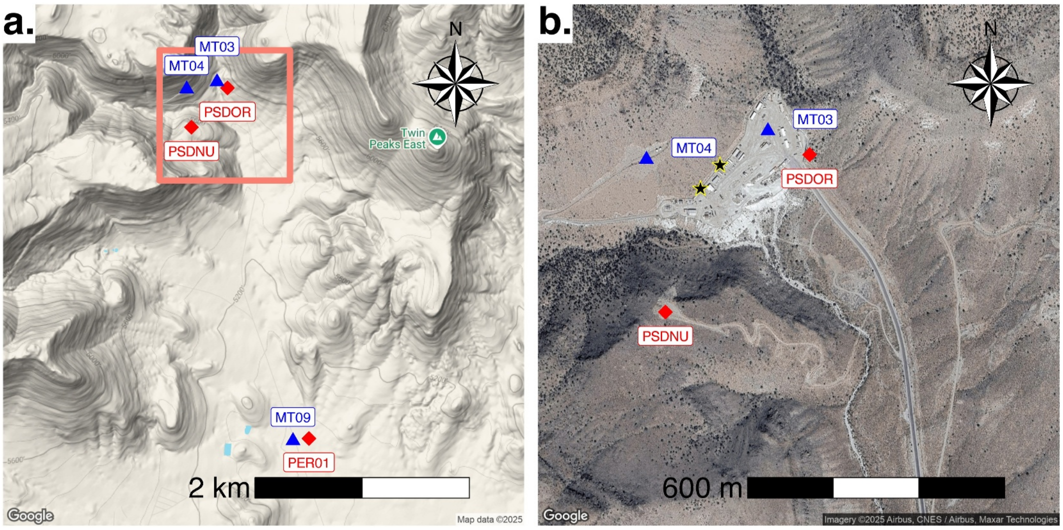

Figure 1. A map of the study area. Infrasound stations are red diamonds and sonic anemometers are blue triangles. Stars denote the entrances to an underground complex.

dates. The median works better than the mean because wind speed creates order of magnitude variations in pressure signals on infrasound sensors, so an outlier-insensitive method was necessary.

We then constructed circular spectrograms to visualize power variations with respect to frequency and time of day. In these plots, a pixel's angular position represents time of day and distance from the center represents frequency. The color of each pixel is set to the median power of that time-frequency bin (Figure 2). The resulting plots showcase daily trends in acoustic power that would be more difficult to visualize using a more typical rectangular spectrogram. We then selected spectra for a 10 min period starting at 1930 UTC for each day in the month of November (approximate solar noon), 0730 UTC (approximate solar midnight) and 1600 UTC (about two hours after dawn). The median for each station, split across weekdays and weekends, is shown in Figure 3.

We used a network of meteorological stations to assess winds in the vicinity of the microbarometers. These stations acquired wind speed and direction using 3D sonic anemometry at a 10 Hz sampling rate and at a height of 10 m above the ground. A comprehensive description of this sensor network is provided in Wharton et al. (2023). Two of the anemometers, MT03 and MT09, were within 200 m of acoustic sensors PSDOR and PER01 respectively (Figure 1a). The third anemometer, MT04, was located on a mesa slope across a small canyon about 360 m from acoustic sensor PSDNU (Figure 1b). We note that, while MT03 and MT04 are separated by a distance of less than 350 m, the local terrain features produce strong wind variations (in both speed and direction) between the two sites. MT04 experiences both diurnally driven upslope and downslope flows along the mesa as well as channeled downvalley flows from the adjoining west-east running side canyon. MT03 generally sees diurnal upvalley and downvalley flows from the north-south running side canyon on the eastern side of the tunnel apron. MT09, on the otherhand, is influenced strongly by the larger-scale diurnal upvalley and downvalley winds from the Yucca Flat valley (Wharton et al., 2023). Similar to the acoustic data, we separated the wind speed data into ten-minute sections and displayed the resulting wind speed variability in circular plots (Figure 4).

3. Results and Discussion

Across all stations, there are two distinct drops in noise below 10 Hz: one at local sunset, 0000–0100 UTC, and another after local sunrise, 1400–1700 UTC (Figure 2). These drops occur at the same time as daily wind lulls measured at nearby anemometers (Figure 4; also see Wharton et al. (2023)). Noise below 10 Hz is highest during the day for stations PER01 (Figures 3a and 3b) and PSDNU (Figures 3c and 3d) and it is the highest during the night for the station PSDOR (Figures 3e and 3f). The anemometer at MT03 records higher winds at night (Figure 4a), as this station is at the terminus of a north-south running side canyon and the nighttime northerly flows are channeled and strengthened as they reach the sonic anemometer site. This is consistent with the low frequency noise patterns seen on the microbarometer at PSDOR. The other anemometer/microbarometer patterns

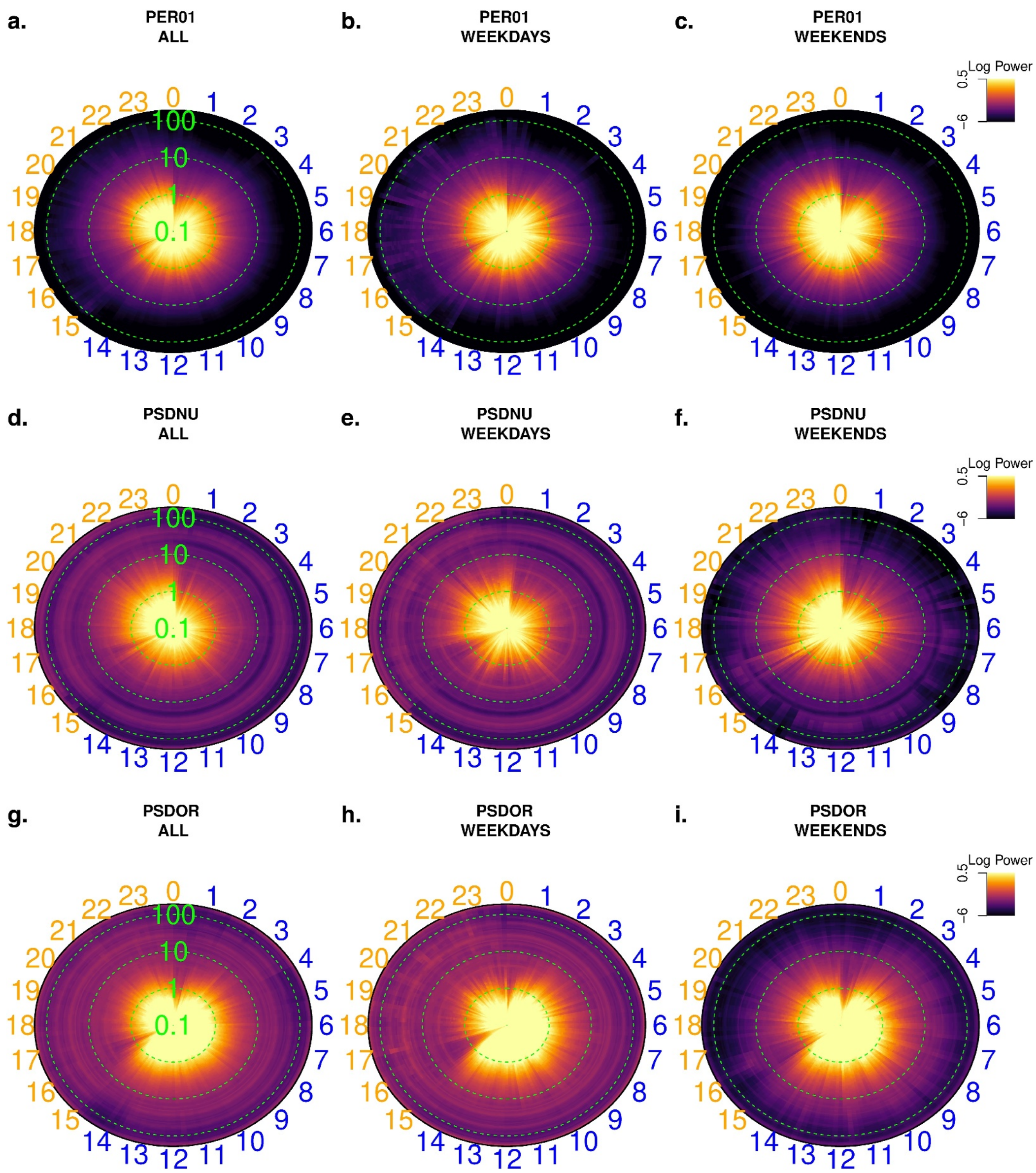

Figure 2. Circular spectrograms showing median daily power levels at three infrasound stations separated into weekends and weekdays. Frequency is measured from the center to the outer edge of the circle, starting at 0.1 Hz and ending at 200 Hz. The radial axis is log-scaled. The color scale is in log power (Pa^2Hz^{-1}). The outer numbers are UTC hour, colored blue for night and orange for day.

are less dramatic: wind levels at MT04 (closest to PSDNU) are similar during the daylight and the nighttime hours due to the location of the anemometer which experiences relatively weaker upslope and downslope flows (Figure 4b). Likewise winds at MT09 (closest to PER01) are at similar intensities at local noon and midnight, though stronger than at MT03 (Figure 4c). The observed sunrise and sunset wind lulls (and resulting lower levels of broadband noise on the microbarometers) is consistent with thermally driven winds over sloping terrain (Farina & Zardi, 2023). A period of low wind speed in the morning hours is often observed under fair skies in mountain valleys (e.g. Brötz et al., 2014; Nadeau et al., 2020). Another period of low wind speed occurs in the evening, when the reduction in solar flux leads a drop in turbulence and the development of the nocturnal boundary layer (Nadeau et al., 2011; Sastre et al., 2015). Later in the night, topographically complex regions can experience katabatic, or downslope, winds driven by radiative cooling. During the day, areas with rugged topography may experience anabatic, or upslope, winds driven by solar heating. Thus, topography strongly controls the structure

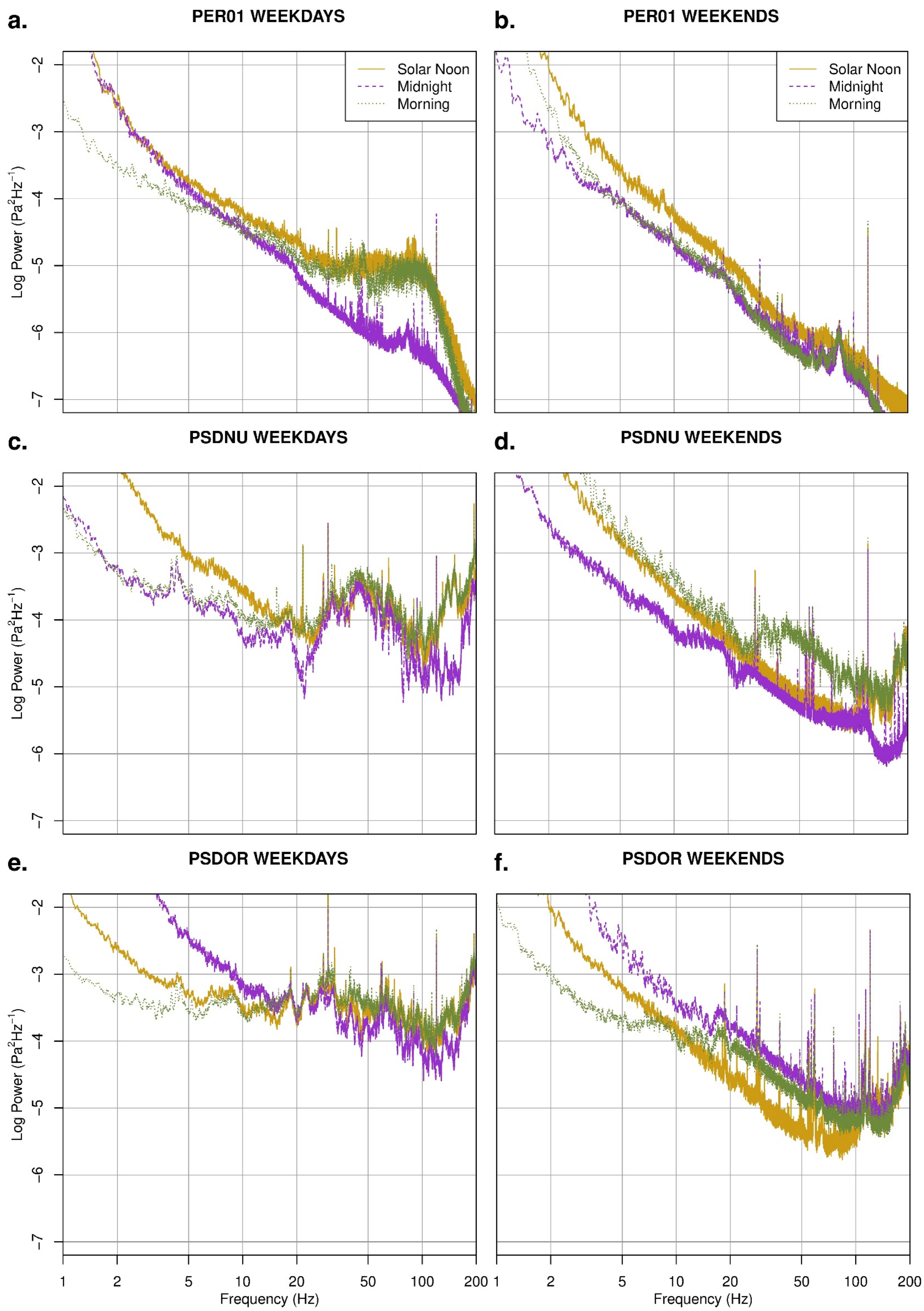

Figure 3. Median daily spectra for each station calculated for solar noon, midnight, and about 2 hours after dawn.

of these winds. This was further highlighted during tracer release experiments conducted at the same underground facility; the terrain is particularly complex as side canyons and slopes are both perpendicular and parallel to the background wind regime, which both accelerates and decelerates the wind speed over small ground distances

10.1029/2025GL116415

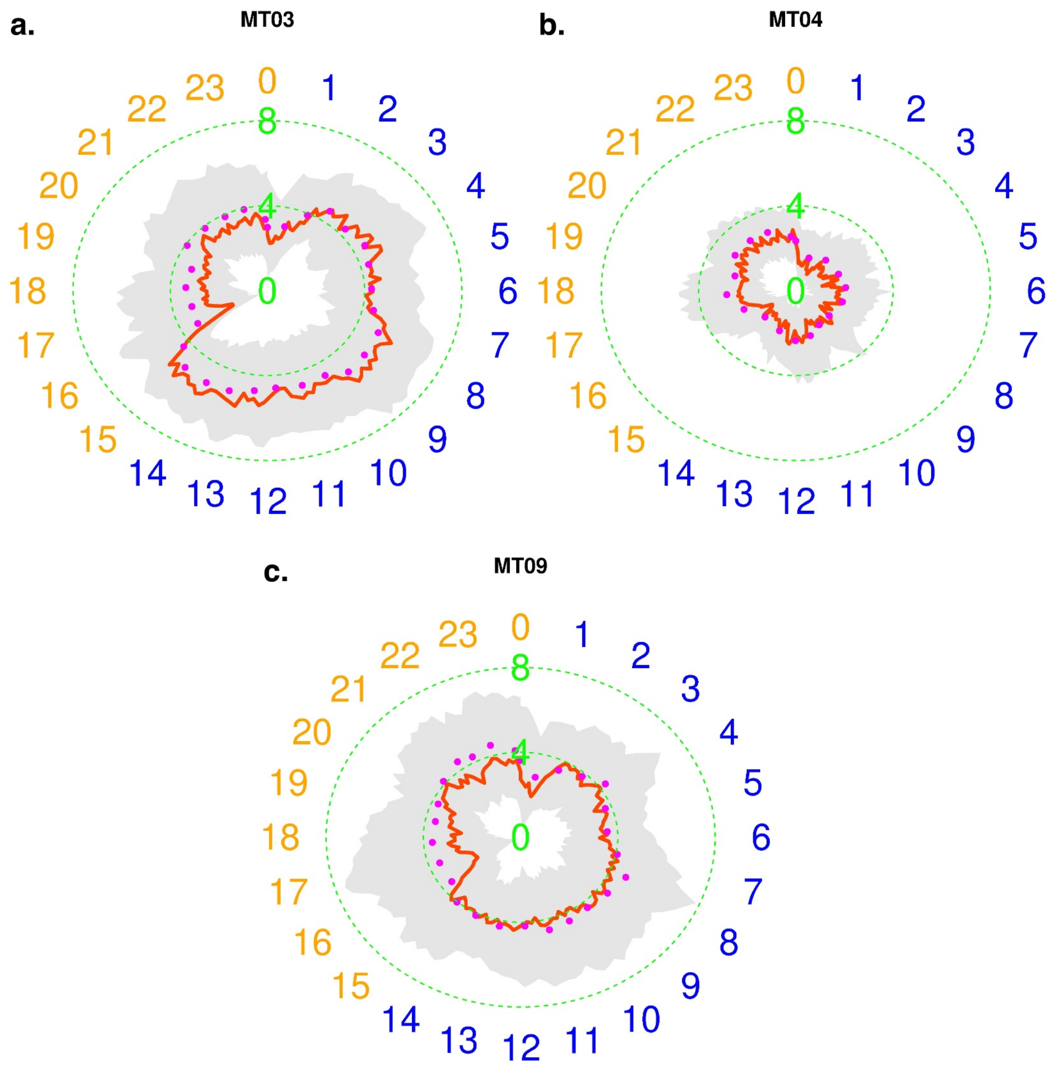

Figure 4. Circular plots showing the median wind speed (solid line), mean wind speed (dotted line), and standard deviation (gray regions) for the month of November. Wind speed is measured from the center to the outer edge of the circle, starting at 0 m/s and ending at 8 m/s. The outer numbers are UTC hour (blue for night and orange for day).

(Wharton et al., 2023). It also is consistent with results from field campaigns in other locations as well (Farina & Zardi, 2023).

In general, the geophysical acoustics community assumes that wind noise will be high during the day and low during the night (Walker & Hedlin, 2010). Global surveys of wind noise generally support this, although they note that interference levels are highly variable by location and time of year (e.g. J. R. Bowman et al. (2005)). Our study shows that wind noise over a topographically complex site can vary in both intensity and timing over scales as small as hundreds of meters. For example, the station PSDOR (at the opening of a narrow canyon) experiences much higher winds at night than the station PSDNU (600 m away on a ridge).

The station PER01 had elevated noise between 10 and 100 Hz during daylight hours on weekdays, but not at night or weekends (Figures 2a–2c, top row). A spectrum taken at solar noon for weekdays at PER01 shows a corresponding power enhancement between ≈30–100 Hz (Figures 3a and 3b). This pattern of activity is consistent with highway traffic on the tunnel access road that passes just to the west of the station. Highway road noise creates a broad spectral peak starting from 10s of Hz, peaking at about 1000 Hz, and decreasing thereafter (Rochat & Reiter, 2016). From the perspective of infrasound sensors that typically sample at <1000 Hz, this would produce a "blue" noise spectrum (increasing with frequency) as opposed to a more typical "red" noise spectrum from sources such as wind. We hypothesize that a high-frequency enriched traffic noise spectrum superimposed on a high-frequency deficient wind noise spectrum explains the daytime weekday enhancement at PER01.

The stations PSDNU and PSDOR record enhanced power above 20 Hz both during the day and night on weekdays, but not on weekends (Figures 2d–2i and 3c–3f). Since the facility near these stations is not occupied at night, this enhanced power is unlikely to be related to vehicle traffic or construction activities. Rather, it likely reflects the underground ventilation system, which is run 24 hr a day on weekdays, but shut off on weekends. The ventilation system is clearly audible to humans at a distance of hundreds of meters from the tunnel entrance. It consists of fans and ductwork similar to but on a much larger scale than commercial and residential Heating, Ventilation, and Cooling (HVAC) systems. HVAC systems produce powerful sound in the tens to hundreds of Hz (Thakre & Vijay, 2024) with both broadband and narrowband frequency components (Guedel, 2005). Thus, this single source dominates the acoustic background above about 20 Hz during the week for the two stations within several hundred meters. The slightly enhanced noise levels on weekdays at solar noon between 20 and 100 Hz (Figures 3a, 3c, and 3e) could represent vehicle activity at the facility, similar to the road noise observed at PER01. Finally, we speculate that the presence of hourly pulses of broadband activity during weekdays at PSDOR (Figure 2h) may correspond with periodic entry and exit of the tunnel locomotive.

There are some narrowband signatures that show up on all three stations continuously. The most prominent of these are present at 30, 60, and 120 Hz. These are likely the result of nearby transformers and power lines, which can produce acoustic emissions at multiples of their modulation frequency (Lu et al., 2025). In addition, electromagnetic interference can couple directly into sensor cables, producing spurious signals (D. C. Bowman et al., 2019). All three stations are close to power lines and/or facilities powered using alternating current, indicating that electromagnetic interference cannot be eliminated as a potential source. However, the acoustic emissions from power lines and transformers may be contributing as well.

4. Conclusion

Analysis of microbarometer data recordings using a circular spectrogram provided insights into the different noise trends influenced by topography and human activity. We identified diurnal variations driven by micrometeorological factors, as well as daily and weekly cycles linked to anthropogenic influences. Diurnal trends related to katabatic and anabatic winds appear to be influenced by topography, with noise levels being the lowest at sunrise and sunset. Wind presents as low frequency broadband noise mainly in the 0.1–10 Hz band. Anthropogenic activity is most evident above 10 Hz. Narrowband features present at all hours during the work week are likely from ventilation systems, while narrowband features that persist through the weekend are probably from electrical systems. Our study shows that wind noise over a topographically complex site can vary in both intensity and timing over a range of hundreds of meters. This underscores the need for careful site selection before emplacing infrasound sensors for data collection, and perhaps suggests that there would be merit in conducting pre-deployment wind speed survey prior to deploying infrasound sensors. This is standard practice for certain globe-spanning permanent infrasound arrays (Ken Macpherson, personal communication), but we highlight that this siting is important for more temporary deployments as well. Facilities, roads, etc. can be a major noise source as well, and their interference varies on different time scales depending on the type of emitter. Microscale meteorological simulations of the deployment location showed promise in evaluating wind speed trends (Wiersema et al., 2023), suggesting that they could be a useful tool for site selection in the future. We hope that the findings in this study will provide a useful guide for researchers who aim to deploy their own networks in unique topographic settings in areas with significant human activity.

Data Availability Statement

Data from the Physics Experiment 1 acoustic sensor network and meteorological tower stations were used in the creation of this manuscript. A report titled "A Multi-Physics Experiment for Low-Yield Nuclear Explosion Monitoring" (Myers et al., 2024) describes the experiment and associated data products. These data are presently restricted to U.S. government researchers and are not accessible to the public. Data is anticipated to be released at least 2 years after the end of the experiment. Data analysis andFigure generation was performed using the *stringr* (Wickham, 2023), *lubridate* (Grolemund & Wickham, 2011), *colormap* (Karambelkar, 2016) and *RSEIS* (Lees & Harris, 2024) packages in *R*. Figure 1 was generated using the *ggmap* (Kahle & Wickham, 2013), the *ggspatial*

(Dunnington, 2023), the *ggstar* (Xu, 2022) and the *XLConnect* packages (Mirai Solutions GmbH, 2024) in *R*. All of these *R* packages are available on the Comprehensive R Archive Network (CRAN; https://cran.r-project.org/). Figure manipulation utilized the *ImageMagick* software suite (ImageMagick Studio LLC, 2023).

Acknowledgments

The PE1 Experiment Team consists of the full author list in Myers et al. (2024) (https://doi.org/10.2172/2345984). The authors thank Jerry Rouse for his edits on an early draft of the paper. They also thank Ken Macpherson and an anonymous reviewer for their constructive comments during the peer review process. Sandia National Laboratories is a multi-mission laboratory managed and operated by National Technology & Engineering Solutions of Sandia, LLC (NTESS), a wholly owned subsidiary of Honeywell International Inc., for the U.S. Department of Energy's National Nuclear Security Administration (DOE/NNSA) under Contract DE-NA0003525. This written work is authored by an employee of NTESS. The employee, not NTESS, owns the right, title and interest in and to the written work and is responsible for its contents. Any subjective views or opinions that might be expressed in the written work do not necessarily represent the views of the U.S. Government. The publisher acknowledges that the U.S. Government retains a non-exclusive, paid-up, irrevocable, world-wide license to publish or reproduce the published form of this written work or allow others to do so, for U.S. Government purposes. The DOE will provide public access to results of federally sponsored research in accordance with the DOE Public Access Plan. This work was also performed under the auspices of the U. S. Department of Energy by Lawrence Livermore National Laboratory under Contract DE-AC52-07NA27344. This work was also performed by Pacific Northwest National Laboratory (PNNL), which is operated by Battelle for the U. S. Department of Energy under contract DE-AC05-76RL01830. This work was also done by Mission Support and Test Services, LLC, Under Contract No. DE-NA0003624 with the U.S. Department of Energy, and the Office of Defense Nuclear Nonproliferation Research and Development.

References

Albert, D. G., & Decato, S. N. (2017). Acoustic and seismic ambient noise measurements in urban and rural areas. *Applied Acoustics*, *119*, 135–143. https://doi.org/10.1016/j.apacoust.2016.12.015

Albert, S. A., Pankow, K., & Berg, E. M. (2021). *Comparison of infrasound noise reduction systems for use in temporary deployments (techreport)*. Sandia National Laboratories. (SAND2021-10136).

Bird, E., Bowman, D. C., Seastrand, D. R., Wright, M. A., Lees, J. M., & Dannemann Dugick, F. K. (2021). Monitoring changes in human activity during the COVID-19 shutdown in Las Vegas using infrasound microbarometers. *Journal of the Acoustical Society of America*, *149*(3), 1796–1802. https://doi.org/10.1121/10.0003777

Bowman, D. C., Lees, J. M., Cutts, J. A., Komjathy, A., Young, E. F., Seiffert, K. T., et al. (2019). Geoacoustic observations on drifting balloon-borne sensors. In A. Le Pichon, E. Blanc, & A. Hauchecorne (Eds.), *Infrasound monitoring for atmospheric studies: Challenges in middle-atmosphere dynamics and societal benefits* (pp. 125–171). Springer Nature.

Bowman, J. R., Baker, G. E., & Bahavar, M. (2005). Ambient infrasound noise. *Geophysical Research Letters*, *32*(9), L09803. https://doi.org/10.1029/2005GL022486

Brötz, B., Eigenmann, R., Dörnbrack, A., Foken, T., & Wirth, V. (2014). Early-morning flow transition in a valley in low-mountain terrain under clear-sky conditions. *Boundary-Layer Meteorology*, *152*(1), 45–63. https://doi.org/10.1007/s10546-014-9921-7

Brown, D., Ceranna, L., Prior, M., Mialle, P., & Le Bras, R. (2014). The IDC seismic, hydroacoustic and infrasound global low and high noise models. *Pure and Applied Geophysics*, *171*(3–5), 361–375. https://doi.org/10.1007/s00024-012-0573-6

Campus, P., & Christie, D. R. (2010). Worldwide observations of infrasonic waves. In A. Le Pichon, E. Blanc, & A. Hauchecorne (Eds.), *Infrasound monitoring for atmospheric studies* (pp. 185–234). Springer Science and Business Media.

Dunnington, D. (2023). ggspatial: Spatial data framework for ggplot2 [Computer software manual]. Retrieved from https://CRAN.R-project.org/package=ggspatial(Rpackageversion1.1.9

Farina, S., & Zardi, D. (2023). Understanding thermally driven slope winds: Recent advances and open questions. *Boundary-Layer Meteorology*, *189*(1–3), 5–52. https://doi.org/10.1007/s10546-023-00821-1

Frisk, G. V. (2012). Noiseonomics: The relationship between ambient noise levels in the sea and global economic trends. *Scientific Reports*, *2*(1), 437. https://doi.org/10.1038/srep00437

Grolemund, G., & Wickham, H. (2011). Dates and times made easy with lubridate. *Journal of Statistical Software*, *40*(3), 1–25. https://doi.org/10.18637/jss.v040.i03

Guedel, A. (2005). *Aerodynamic noise of fans (techreport No. AIVC-CR01)*. Air Infiltration and Ventilation Centre.

Hupe, P., Ceranna, L., Le Pichon, A., Matoza, R. S., & Mialle, P. (2022). International Monitoring System infrasound data products for atmospheric studies and civilan applications. *Earth System Science Data*, *14*(9), 4201–4230. https://doi.org/10.5194/essd-14-4201-2022

ImageMagick Studio LLC. (2023). Imagemagick. Retrieved from https://imagemagick.org

Kahle, D., & Wickham, H. (2013). ggmap: Spatial visualization with ggplot2. *The R Journal*, *5*(1), 144–161. https://doi.org/10.32614/rj-2013-014

Karambelkar, B. (2016). colormap: Color palettes using colormaps node module. *[Computer software manual]*. Retrieved from https://CRAN.R-project.org/package=colormap(Rpackageversion0.1.4

Koch, K., & Pilger, C. (2019). Infrasound observations from the site of past underground nuclear explosions in North Korea. *Geophysical Journal International*, *216*(1), 182–200. https://doi.org/10.1093/gji/ggy38

Lees, J. M., & Harris, D. (2024). Rseis: Seismic time series analysis tools [Computer software manual]. Retrieved from https://CRAN.R-project.org/package=RSEIS(Rpackageversion4.2-4

Lees, J. M., & Park, J. (1995). Multiple-taper spectral analysis: A stand-alone C-subroutine. *Computers & Geosciences*, *21*(2), 199–236. https://doi.org/10.1016/0098-3004(94)00067-5

Lu, Y., Wu, S. F., Nie, C., & He, W. (2025). Locating and reconstructing transformer low-frequency noises with a 3D, six-microphone array. *Applied Acoustics*, *228*, 110351. https://doi.org/10.1016/j.apacoust.2024.110351

Macpherson, K. A., Coffey, J. R., Witsil, A. J., Fee, D., Holtkamp, S., Dalton, S., et al. (2022). Ambient infrasound noise, station performance, and their relation to land cover across Alaska. *Seismological Research Letters*, *93*(4), 2239–2258. https://doi.org/10.1785/0220210365

Mirai Solutions GmbH. (2024). Xlconnect: Excel connector for r [Computer software manual]. Retrieved from https://CRAN.R-project.org/package=XLConnect(Rpackageversion1.1.0

Myers, S. C., Abbott, G., Alexander, T., Alger, E., Alvarez, A., Annabelle, N., et al. (2024). *A multi-physics experiment for low-yield nuclear explosion monitoring (techreport No. LLNL-TR-864107)*. Lawrence Livermore National Laboratory. https://doi.org/10.2172/2345984

Nadeau, D. F., Oldroyd, H. J., Pardyjak, E. R., Sommer, N., Hoch, S. W., & Parlange, M. B. (2020). Field observations of the morning transition over a sleep slope in a narrow alpine valley. *Environmental Fluid Mechanics*, *20*(5), 1199–1220. https://doi.org/10.1007/s10652-018-9582-z

Nadeau, D. F., Pardyjak, E. R., Higgins, C. W., Fernando, H. J. S., & Paralnge, M. B. (2011). A simple model for the afternoon and early evening decay of convective turbulence over different land surfaces. *Boundary-Layer Meteorology*, *141*(2), 301–324. https://doi.org/10.1007/s10546-011-9645-x

Park, J., Che, I.-Y., Stump, B., Hayward, C., Dannemann, F., Jeong, S., et al. (2018). Characteristics of infrasound signals from North Korean underground nuclear explosions on 2016 January 6 and September 9. *Geophysical Journal International*, *214*(3), 1865–1885. https://doi.org/10.1093/gji/ggy252

Pryor, S. C., Barthelmie, R. J., Bukovsky, M. S., Leung, L. R., & Sakaguchi, K. (2020). Climate change impacts on wind power generation. *Nature Reviews Earth & Environment*, *1*(12), 627–643. https://doi.org/10.1038/s43017-020-0101-7

Raspet, R., Abbott, J.-P., Webster, J., Yu, J., Talmadge, K. C., Collier, S., & Noble, J. (2019). New systems for wind noise reduction for infrasonic measurements. In A. Le Pichon, E. Blanc, & A. Hauchecorne (Eds.), *Infrasound monitoring for atmospheric studies* (2nd ed., pp. 91–124). Springer Nature.

Ripepe, M., Marchetti, E., Delle Donne, D., Genco, R., Innocenti, L., Lacanna, G., & Valade, S. (2018). Infrasonic early warning systems for explosive eruptions. *Journal of Geophysical Research: Solid Earth*, *123*(11), 9570–9585. https://doi.org/10.1029/2018JB015561

Rochat, J. L., & Reiter, D. (2016). Highway traffic noise. *Acoustics Today*, *12*(4), 38–47.

Sastre, M., Yagüe, C., Román-Cascón, C., & Maqueda, G. (2015). Atmospheric boundary-layer evening transitions: A comparison between two different experimental sites. *Boundary-Layer Meteorology*, *157*(3), 375–399. https://doi.org/10.1007/s10546-015-0065-1
Thakre, C., & Vijay, R. (2024). Impact of low-frequency noise on a residential zone due to commercial HVAC systems. *Journal of Building Engineering*, *91*, 109616. https://doi.org/10.1016/j.jobe.2024.109616
Walker, K. T., & Hedlin, M. A. (2010). A review of wind-noise reduction technologies. In *Infrasound monitoring for atmospheric studies* (pp. 141–182). Springer Science and Business Media.
Wharton, S., Brown, M. J., Dexheimer, D., Fast, J. D., Newsom, R. K., Schalk, W. K., & Wiersema, D. J. (2023). Capturing plume behavior in complex terrain: An overview of the Nevada National Security Site Meteorological Experiment (METEX21). *Frontiers in Earth Science*, *11*, 1251153. https://doi.org/10.3389/feart.2023.1251153
Wickham, H. (2023). stringr: Simple, consistent wrappers for common string operations [Computer software manual]. Retrieved from https://CRAN.R-project.org/package=stringr(Rpackageversion1.5.1
Wiersema, D. J., Wharton, S., Arthur, R. S., Juliano, T. W., Lundquist, K. A., Glascoe, L. G., et al. (2023). Assessing turbulence and mixing parameterizations in the gray-zone of multiscale simulations over mountainous terrain during the METEX21 field experiment. *Frontiers in Earth Science*, *11*, 1251180. https://doi.org/10.3389/feart.2023.1251180
Wynn, N. R., & Dannemann Dugick, F. K. (2023). Modeling and characterizing urban infrasonic and low-frequency noise in the Las Vegas, NV region. *Journal of the Acoustical Society of America*, *154*(3), 1439–1447. https://doi.org/10.1121/10.0020837
Xu, S. (2022). ggstar: Multiple geometric shape point layer for "ggplot2" [Computer software manual]. Retrieved from https://CRAN.R-project.org/package=ggstar(Rpackageversion1.0.4
Zhang, A., Yang, J., Luo, Y., & Fan, S. (2023). Forecasting the progression of human civilization on the Kardashev Scale through 2060 with a machine learning approach. *Scientific Reports*, *13*(1), 11305. https://doi.org/10.1038/s41598-023-38351-y